Integrated migration and internal multiple elimination

Kees Wapenaar, Jan Thorbecke, Joost van der Neut and Evert Slob, Delft University of Technology,*
Filippo Broggini, Jyoti Behura and Roel Snieder, Colorado School of Mines

SUMMARY

Standard seismic migration, applied to data with internal multiples, leads to images with ghosts. The reason is that one-way wave field extrapolation operators give erroneous downgoing and upgoing fields in the subsurface, which in the correlation process lead to ghosts. By using "data-driven wave field reconstruction" it is possible to obtain the correct downgoing and upgoing wave fields in the subsurface. Using these in the correlation process leads to ghost-free images.

INTRODUCTION

Standard seismic depth migration involves one-way downward extrapolation of downgoing and upgoing wave fields from the acquisition surface to a depth level in the subsurface, correlating the downward extrapolated downgoing and upgoing fields and selecting the $t = 0$ component to get an image of the reflectivity at the chosen depth level (Claerbout, 1971; Berkhout, 1982). By repeating this procedure for all depth levels of interest, a reflectivity image of the subsurface is obtained. Migrated data usually suffer from ghost images due to multiple reflections. Assuming the surface-related multiples are suppressed prior to migration (Verschuur et al., 1992), those ghost images are caused by the internal multiples (e.g. event 3 in Figures 1b and c).

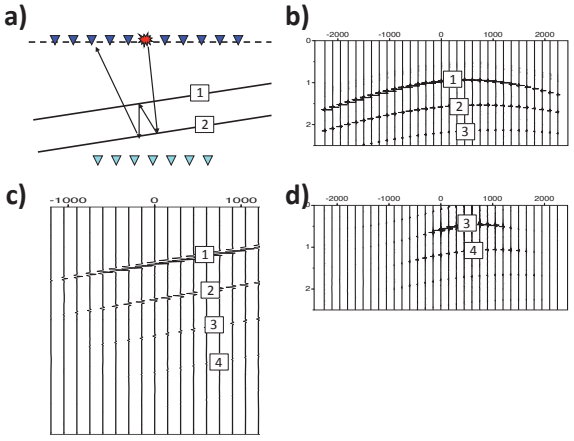

Fig. 1: *Example of standard depth migration. (a) Medium with two dipping interfaces. (b) Reflection response at the surface (one shot record). (c) Migration result with ghosts. (d) Downward extrapolated upgoing wave field at virtual receivers (light-blue triangles in Fig. a) below the deepest interface.*

The obvious explanation is that a standard depth migration scheme cannot distinguish primaries from multiply reflected waves, hence, a multiply reflected event from a relatively shallow interface (as indicated by the raypath in Figure 1a) is interpreted as a primary reflection from a deeper interface and thus erroneously imaged at a too large depth. Another way of explaining the same phenomenon is that one-way downward extrapolation operators yield erroneous downgoing and upgoing waved fields at depth. For example, Figure 1d shows the downward extrapolated upgoing wave field at the virtual receivers (the light-blue triangles in Figure 1a) below the deepest interface. Because the source is at the surface there can only be downgoing waves below the deepest interface, hence, the upgoing field in Figure 1d should be zero. The erroneous non-zero field correlates with the downgoing field below the deepest reflector and gives rise to the ghost images in Figure 1c.

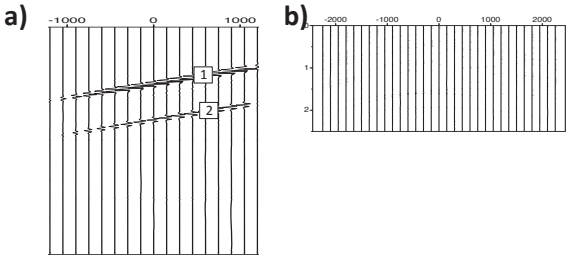

Fig. 2: *Example of proposed migration scheme. (a) Migration result. (b) Downward extrapolated upgoing wave field at virtual receivers below the deepest interface.*

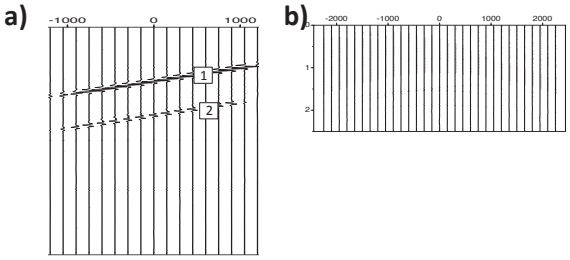

Fig. 3: *As Figure 2, but using a velocity with 5% velocity error.*

Here we introduce a new approach to deal with internal multiple reflections in depth migration. The main idea is that we replace the independent one-way extrapolation operators for downgoing and upgoing waves by a new downward extrapolation scheme that gives the correct downward and upward propagating fields at depth, due to sources at the surface (hence, for the example in Figure 1 this scheme gives a zero upgoing wave field below the deepest reflector, see Figure 2b). A ghost-free image is obtained by correlating the correct downgoing and upgoing fields at depth, followed by selecting the $t = 0$ component (and repeating the whole procedure for all depth levels of interest), see Figure 2a. Following this approach, not only the ghost images are suppressed, but in addition the multiples in the extrapolated downgoing and upgoing fields at depth contribute to the primary image. This approach is stable with respect to errors in the macro velocity model (Figure 3). Like in standard depth migration, velocity errors cause mispositioning of reflectors and defocusing of diffractors, but the ghost suppression is not affected by these errors.

DOI http://dx.doi.org/10.1190/segam2012-1298.1

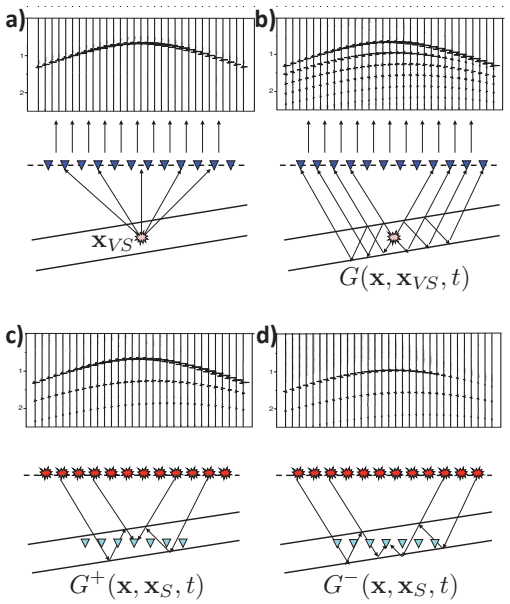

Fig. 4: *Data-driven "wave field reconstruction" (Broggini et al., 2011; Wapenaar et al., 2011a) uses the reflection response at the surface and an estimate of the first arrivals (a) to obtain the full response to a virtual source in the subsurface (b). Using reciprocity and decomposition, this response is turned into the downgoing (c) and upgoing (d) fields in the suburface, due to sources at the surface. These are the fields that are needed to form a ghost-free image of the subsurface.*

DOWNWARD WAVE FIELD EXTRAPOLATION

A possible method to obtain the correct downward and upward propagating fields at depth is two-way wave field extrapolation, followed by up/down decomposition. We showed previously that this leads in principle to ghost-free images (Wapenaar et al., 1987). However, we did not pursue this approach because of the high sensitivity of the two-way extrapolation operator with respect to errors in the macro velocity model. Ideally we would like to use a downward extrapolation scheme that is not more sensitive to errors in the macro velocity model than the one-way operators used in standard depth migration. The data-driven "wave field reconstruction method" that we introduced last year (Broggini et al., 2011; Wapenaar et al., 2011a) provides the required operator. Recall that this method uses the reflection data at the surface (Figure 1b) and an estimate of the first arrivals from a virtual source in the subsurface (Figure 4a) to obtain the full response at the surface to a virtual source in the subsurface (Figure 4b). In the terminology of depth migration, an "estimate of the first arrivals from a virtual source in the subsurface" is nothing but the "one-way extrapolation operator in the macro velocity model". Similarly, the "full response at the surface to a virtual source in the subsurface" is, via reciprocity, nothing but the "total field at depth, due to sources at the surface". Hence, the wave field reconstruction method actually applies a one-way operator defined in a macro model (Figure 4a) to the reflection data at the surface (Figure 1b) and gives the total field at depth (Figure 4b, with reciprocity applied). Two different versions of the scheme exist, one giving the total field observed by a monopole receiver and the other by a dipole-type receiver. By subtracting and adding these responses, respectively, the total field is decomposed into the required downgoing and upgoing wave fields at depth (Figure 4c,d). In the following we show step-by-step how the downgoing and upgoing wave fields in Figure 4c,d are obtained from the reflection data at the surface and how these fields (for all depth levels of interest) are used to form the ghost-free image of the subsurface (Figure 2a).

CREATING THE VIRTUAL-SOURCE RESPONSE

We discuss the procedure by which the virtual-source response of Figure 4b is obtained from the reflection data at the surface (Figure 1b).

The medium configuration

The medium configuration in Figures 1a and 4 is defined as follows. The reflection-free acquisition surface is located at $z = 0$. The first reflector is defined as $z = z_1 - ax$, with $z_1 = 1000$ m and $a = 1/4$. The second reflector is parallel to the first reflector and the layer thickness is 618 m. The virtual source in Figure 4a,b is defined at $\mathbf{x}_{VS} = (x_{VS}, z_{VS}) = (0, 1320)$ m. The velocity is constant throughout the medium (2000 m/s), and the densities of the different layers are 1000, 5000 and 1000 kg/m^3. Furthermore the medium is lossless. For this medium we previously analyzed the creation of the virtual-source response by the method of stationary phase (Wapenaar et al., 2012). The velocity was chosen constant to facilitate this analysis, but the method we discuss here is also valid for variable velocity media (for a numerical experiment in a variable-velocity syncline model, see Broggini et al., 2012). In the following numerical experiment we use the constant velocity model, so that the results can easily be compared with our earlier analytical result. The sources at the surface are located between -1100 and 1100 m and the receivers between -2250 and 2250 m. The source and receiver spacing is 10 m.

Initiating the iterative process

The iterative procedure is a 2D extension of the iterative 1D scheme discussed by Rose (2002) and Broggini et al. (2011). Figure 5b shows again the direct arrivals of the virtual source at $\mathbf{x}_{VS}$ in the subsurface. These direct arrivals are reversed in time, which turns the upgoing field at the surface $z = 0$ into a downgoing field $p_0^+(\mathbf{x}, t)$, see Figure 5a. The red curves along these events define a window function $w(\mathbf{x}, t)$, which equals 1 between these curves and 0 elsewhere. This window will be used later. The field $p_0^+(\mathbf{x}, t)$ is used as the initial downgoing field at the surface $z = 0$, which illuminates the medium from above (Figure 5c). The response to this field is obtained by convolving it with the reflection response of the medium, according to

$$p_0^-(\mathbf{x}_R, t) = \int_{-\infty}^{\infty} \left[R(\mathbf{x}_R, \mathbf{x}, t) * p_0^+(\mathbf{x}, t)\right]_{z=0} \mathrm{d}x, \qquad (1)$$

for $z_R = 0$. In practical situations, $R(\mathbf{x}_R, \mathbf{x}, t)$ is the measured reflection response, after surface-related multiple elimination and deconvolution for the source wavelet. For this example we use a numerically modeled reflection response (Figure 1b). Equation 1 is evaluated numerically as well. The result of this convolution is the upgoing wave field $p_0^-(\mathbf{x}, t)$ at the surface, see Figure 5d.

The iterative process

Next, we apply an iterative scheme, which has the aim to modify the incident field in such a way that, *within the time window, the incident field is equal to minus the time-reversed up-*

DOI http://dx.doi.org/10.1190/segam2012-1298.1

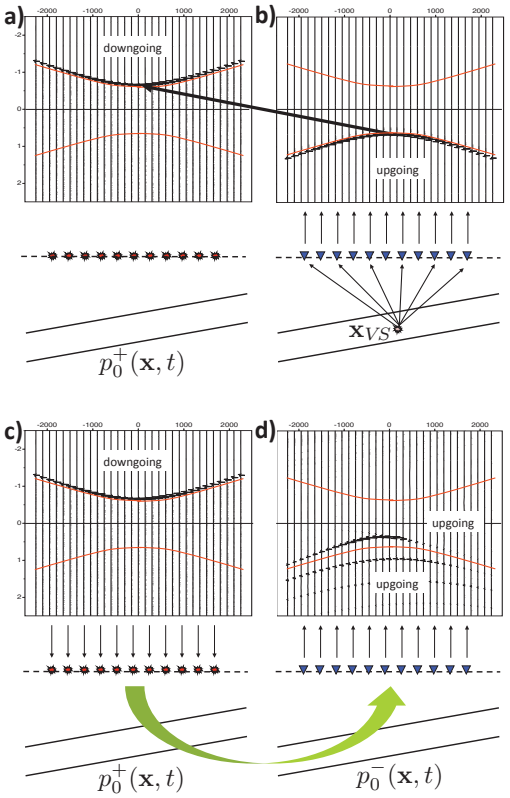

Fig. 5: *Initiating the iterative process. An estimate of the direct field between the virtual source and the surface (b) is reversed in time, giving the initial downgoing field $p_0^+(\mathbf{x},t)$ (a, c). This initial downgoing field $p_0^+(\mathbf{x},t)$ is convolved with the reflection response of the medium, giving the upgoing field $p_0^-(\mathbf{x},t)$ (d).*

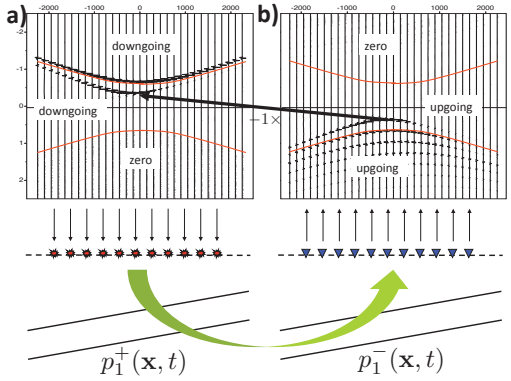

Fig. 6: *The iterative process. The event of the upgoing field between the red curves (b) is reversed in time and subtracted from the initial downgoing field (a). The modified downgoing field $p_k^+(\mathbf{x},t)$ (here $k=1$) is convolved with the reflection response of the medium, giving the modified upgoing field $p_k^-(\mathbf{x},t)$ (b).*

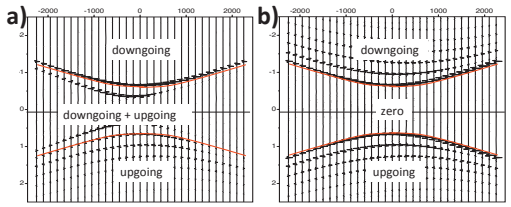

Fig. 7: *Creating the virtual-source response. After finalizing the iterative process, the downgoing and upgoing fields are superposed (a). Next, the total field and its time-reversal are superposed (b). This is interpreted as $G(\mathbf{x},\mathbf{x}_{VS},t) + G(\mathbf{x},\mathbf{x}_{VS},-t)$.*

going field. To achieve this goal, the kth iteration is defined as follows

$$p_k^+(\mathbf{x},t) = p_0^+(\mathbf{x},t) - w(\mathbf{x},t)p_{k-1}^-(\mathbf{x},-t), \quad (2)$$

$$p_k^-(\mathbf{x}_R,t) = \int_{-\infty}^{\infty}\left[R(\mathbf{x}_R,\mathbf{x},t) * p_k^+(\mathbf{x},t)\right]_{z=0}\mathrm{d}x, \quad (3)$$

for $\mathbf{x}$ and $\mathbf{x}_R$ at $z=0$. This scheme starts with $k=1$. The upgoing field $p_0^-(\mathbf{x},t)$ needed in equation 2 is shown in Figure 5d. Only the first event falls within the time window, defined by the red curves. Following equation 2 for $k=1$, we subtract the time-reversal of this event from $p_0^+(\mathbf{x},t)$, which gives the modified incident wave field $p_1^+(\mathbf{x},t)$, see Figure 6a. Using equation 3 we evaluate the reflection response $p_1^-(\mathbf{x},t)$ to this modified incident wave field (Figure 6b). Note that, within the time window, $p_1^-(\mathbf{x},t)$ is identical to $p_0^-(\mathbf{x},t)$ in Figure 5d, hence, further iterations will not cause any changes. Already after one iteration we have achieved the italicized condition mentioned above. This is a consequence of analyzing the simple configuration with two interfaces only. For more complex configurations more iterations will be required.

Creating the virtual-source response

After finalizing the iterative process, we define $p(\mathbf{x},t)$ as the superposition of the final incident and reflected wave fields at $z=0$. Because, for this example, iteration $k=1$ was the final iteration, we have $p(\mathbf{x},t) = p_1^+(\mathbf{x},t) + p_1^-(\mathbf{x},t)$. This total field is shown in Figure 7a. Within the time window this field is antisymmetric in time. Hence, if we superpose the total field and its time-reversed version, i.e., $p_{\mathrm{sym}}(\mathbf{x},t) = p(\mathbf{x},t) + p(\mathbf{x},-t)$, all events within the time window cancel each other, whereas outside the time window this superposition is symmetric, see Figure 7b. Note that, because we consider a lossless medium, $p_{\mathrm{sym}}(\mathbf{x},t)$ obeys the wave equation. Since time-reversal changes the propagation direction, it follows that the causal part is upward propagating at $z=0$ and the acausal part is downward propagating at $z=0$. The first arrival of the causal part of $p_{\mathrm{sym}}(\mathbf{x},t)$ in Figure 7b corresponds with the direct arrival of the response to the virtual source at $\mathbf{x}_{VS}$ (Figure 5b). Given this last observation, combined with the fact that the causal part is upward propagating at $z=0$ and that the total field obeys the wave equation and is symmetric, it is plausible that $p_{\mathrm{sym}}(\mathbf{x},t)$ is proportional to $G(\mathbf{x},\mathbf{x}_{VS},t) + G(\mathbf{x},\mathbf{x}_{VS},-t)$ (where G stands for the Green's function in the real medium). This argumentation holds for more general situations, but it has been checked explicitly

DOI http://dx.doi.org/10.1190/segam2012-1298.1

with the stationary-phase method for the response in Figure 7b (Wapenaar et al., 2012). The causal part of $p_{\rm sym}(\mathbf{x},t)$ in Figure 7b is the virtual-source response that we showed earlier in Figure 4b. It is interpreted as the Green's function $G(\mathbf{x},\mathbf{x}_{VS},t)$. Note that the direct arrival in this retrieved Green's function comes from the initial estimate of the first arrivals (Figure 4a), whereas the internal multiples come entirely from the reflection response (Figure 1b).

DECOMPOSITION

The Green's function $G(\mathbf{x},\mathbf{x}_{VS},t)$ is the response to the virtual source at $\mathbf{x}_{VS}$. In Figure 4b it is clearly seen that this source radiates upward as well as downward propagating fields. The latter arrive at the surface after having been reflected at the interface below the source. We now discuss how the source can be decomposed into an upward and a downward radiating source. To this end we repeat the iterative process, but we replace the minus sign in equation 2 and Figure 6a by a plus sign, hence

$$q_k^+(\mathbf{x},t) = p_0^+(\mathbf{x},t) + w(\mathbf{x},t)q_{k-1}^-(\mathbf{x},-t), \quad (4)$$

$$q_k^-(\mathbf{x}_R,t) = \int_{-\infty}^{\infty}\left[R(\mathbf{x}_R,\mathbf{x},t) * q_k^+(\mathbf{x},t)\right]_{z=0}\mathrm{d}x, \quad (5)$$

with $q_0^-(\mathbf{x},-t) = p_0^-(\mathbf{x},-t)$ following again from equation 1. When this iterative process is finished (here again for $k=1$), we define the total field as $q(\mathbf{x},t) = q_1^+(\mathbf{x},t) + q_1^-(\mathbf{x},t)$, of which the part within the time window is now symmetric in time (instead of antisymmetric). Hence, by evaluating $p_{\rm asym}(\mathbf{x},t) = q(\mathbf{x},t) - q(\mathbf{x},-t)$, all events within the time window again cancel each other (like in Figure 7b), whereas outside the time window this field is antisymmetric. The new created virtual source is therefore also antisymmetric (like a dipole). If we subtract this new response from our retrieved monopole response, i.e., if we evaluate $\frac{1}{2}\{p_{\rm sym}(\mathbf{x},t) - p_{\rm asym}(\mathbf{x},t)\}$ and take the causal part, we obtain the response to an upward radiating virtual source (Figure 8a), whereas the causal part of the superposition $\frac{1}{2}\{p_{\rm sym}(\mathbf{x},t) + p_{\rm asym}(\mathbf{x},t)\}$ yields the response to a downward radiating virtual source (Figure 8b). Using source-receiver reciprocity, a virtual-source response observed by receivers at the surface is equal to the response to sources at the surface, observed by a virtual receiver in the subsurface. Hence, the decomposed responses of Figure 8 are, after applying source-receiver reciprocity, interpreted as the downward and upward propagating fields at a virtual receiver in the subsurface, due to sources at the surface, i.e., as $G^+(\mathbf{x},\mathbf{x}_S,t)$ and $G^-(\mathbf{x},\mathbf{x}_S,t)$, respectively, with $\mathbf{x}$ at the virtual-source depth z_{VS}, see Figure 4c,d. Finally, we used the same procedure to obtain the downgoing and upgoing fields below the second reflector, except that in this case we used 28 iterations (the upgoing field is shown in Figure 2b).

IMAGING WITHOUT GHOSTS

Having obtained the correct downward and upward propagating fields at depth, we are now ready to use these fields for imaging. For a range of virtual receivers at z_{VS}, these fields are related via

$$G^-(\mathbf{x}_R,\mathbf{x}_S,t) = \int_{-\infty}^{\infty}\left[R(\mathbf{x}_R,\mathbf{x},t) * G^+(\mathbf{x},\mathbf{x}_S,t)\right]_{z_{VS}}\mathrm{d}x, \quad (6)$$

for $\mathbf{x}_R$ at z_{VS}. Here $R(\mathbf{x}_R,\mathbf{x},t)$ is the reflection response at the virtual-source depth z_{VS}, for the situation of a homogeneous overburden. It can be resolved from $G^+(\mathbf{x},\mathbf{x}_S,t)$ and $G^-(\mathbf{x},\mathbf{x}_S,t)$ by multidimensional deconvolution (MDD), similar as in seismic interferometry by MDD. To this end, we correlate both sides of equation 6 with the downgoing field and integrate over the sources at the surface. This yields

$$C(\mathbf{x}_R,\mathbf{x}',t) = \int_{-\infty}^{\infty}\left[R(\mathbf{x}_R,\mathbf{x},t) * \Gamma(\mathbf{x},\mathbf{x}',t)\right]_{z_{VS}}\mathrm{d}x, \quad (7)$$

for $\mathbf{x}_R$ and $\mathbf{x}'$ at z_{VS}, with the correlation function and point-spread function defined as

$$C(\mathbf{x}_R,\mathbf{x}',t) = \int_{-\infty}^{\infty} G^-(\mathbf{x}_R,\mathbf{x}_S,t) * G^+(\mathbf{x}',\mathbf{x}_S,-t)\mathrm{d}x_S, \quad (8)$$

$$\Gamma(\mathbf{x},\mathbf{x}',t) = \int_{-\infty}^{\infty} G^+(\mathbf{x},\mathbf{x}_S,t) * G^+(\mathbf{x}',\mathbf{x}_S,-t)\mathrm{d}x_S, \quad (9)$$

respectively (van der Neut et al., 2010; Wapenaar et al., 2011). Inverting equation 7 gives the reflection response $R(\mathbf{x}_R,\mathbf{x},t)$ at depth z_{VS}. This is the ideal approach, which leads to true-amplitude angle-dependent reflection information. A much more simple approach is to evaluate the correlation function via equation 8 for zero-offset and zero time, i.e., $C(\mathbf{x}',\mathbf{x}',0)$, and treat this as an estimate of the reflectivity for all image points $\mathbf{x}'$ of interest. We used an intermediate approach to obtain the image of Figure 2a. We evaluated the correlation function $C(\mathbf{x}_R,\mathbf{x}',t)$ at three depth levels $z_{VS} = 600, 1320, 2150$ m, which are situated above, between and below the two reflectors, respectively, and we applied standard prestack migration to these responses to image the regions between these depth levels. The resulting image of Figure 2a is free of ghosts because we used the correct downgoing and upgoing fields (Figure 4c,d; Figure 2b) in equation 8.

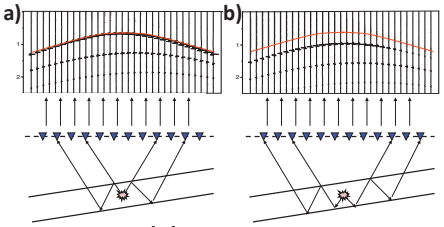

Fig. 8: *Decomposition of the virtual source into an upward (a) and downward (b) radiating source.*

CONCLUSIONS

We have discussed a new approach to integrated migration and internal multiple elimination. The method uses a downward extrapolation scheme that gives the correct downgoing and upgoing wave fields in the subsurface. Like standard migration, the method requires an estimate of the one-way operator, but no knowledge of the reflectors is required; this information comes from the data itself. The method is stable with respect to errors in the macro model (Figure 3). Several other approaches exist that deal with the internal multiple problem (Weglein et al., 1997; Berkhout and Verschuur, 1997; Jakubowicz, 1998; Ten Kroode, 2002). It is beyond the scope of this paper to compare these with our method. We conclude by stating some properties of our proposed scheme. An essential aspect is that we use non-recursive one-way operators, hence, the method does not suffer from error propagation. As a matter of fact, it can start at any desired depth, or be used in a target-oriented approach. Another aspect is that no adaptive prediction and subtraction is required. Last, but not least, the internal multiples contribute to the restoration of the amplitudes of the primary reflections. The effects of triplications, head waves, diving waves, fine-layering etc. need further investigation. A first numerical test with a variable-velocity syncline model shows promising results (Broggini et al., 2012).

DOI http://dx.doi.org/10.1190/segam2012-1298.1

http://dx.doi.org/10.1190/segam2012-1298.1

EDITED REFERENCES

Note: This reference list is a copy-edited version of the reference list submitted by the author. Reference lists for the 2012 SEG Technical Program Expanded Abstracts have been copy edited so that references provided with the online metadata for each paper will achieve a high degree of linking to cited sources that appear on the Web.

REFERENCES

Berkhout, A. J., 1982, Seismic migration: Imaging of acoustic energy by wavefield extrapolation: Elsevier.

Berkhout, A. J. and D. J. Verschuur, 1997, Estimation of multiple scattering by iterative inversion: Part I: Theoretical considerations: Geophysics, **62**, 1586–1595.

Broggini, F., R. Snieder, and K. Wapenaar, 2011, Connection of scattering principles: focusing the wavefield without source or receiver: 81st Annual International Meeting, SEG, Expanded Abstracts, 3845–3850.

Broggini, F., R. Snieder, and K. Wapenaar, 2012, Creating a virtual source inside a medium from reflection data with internal multiples: numerical examples for a laterally-varying velocity model, spatially-extended virtual source, and inaccurate direct arrivals: Presented at the 82nd Annual International Meeting, SEG.

Claerbout, J. F., 1971, Toward a unified theory of reflector mapping: Geophysics, **36**, 467-481.

Jakubowicz, H., 1998, Wave equation prediction and removal of interbed multiples: 68th Annual International Meeting, SEG, Expanded Abstracts, 1527–1530.

Rose, J.H., 2002, 'Single-sided' autofocusing of sound in layered materials: Inverse Problems, **18**, 1923–1934.

Ten Kroode, F., 2002, Prediction of internal multiples: Wave Motion, **35**, 315–338.

van der Neut, J., E. Ruigrok, D. Draganov, and K. Wapenaar, 2010, Retrieving the earth's reflection response by multi-dimensional deconvolution of ambient seismic noise: 72nd Annual International Meeting, SEG, Expanded Abstracts, P406.

Verschuur, D. J., A. J. Berkhout, and C.P.A. Wapenaar, 1992, Adaptive surface-related multiple elimination: Geophysics, **57**, 1166–1177.

Wapenaar, C.P.A., N. A. Kinneging, and A. J. Berkhout, 1987, Principle of prestack migration based on the full elastic two-way wave equation: Geophysics, **52**, 151–173.

Wapenaar, K., F. Broggini, and R. Snieder, 2011a, A proposal for model-independent 3D wave field reconstruction from reflection data: 81st Annual International Meeting, SEG, Expanded Abstracts, 3788–3792.

Wapenaar, K., J. vander Neut, E. Ruigrok, D. Draganov, J. Hunziker, E. Slob, J. Thorbecke, and R. Snieder, 2011b, Seismic interferometry by crosscorrelation and by multidimensional deconvolution: A systematic comparison: Geophysical Journal International, **185**, 1335–1364.

Wapenaar, K., F. Broggini, and R. Snieder, 2012, Creating a virtual source inside a medium from reflection data: a stationary-phase analysis: Geophysical Journal International, in press.

Weglein, A. B., F. A. Gasparotto, P. M. Carvalho, and R. H. Stolt, 1997, An inverse-scattering series method for attenuating multiples in seismic reflection data: Geophysics, **62**, 1975–1989.